Photoluminescence and reversible photo-induced spectral change of $SrTiO_3$



2005 J. Phys.: Condens. Matter 17 923

(http://iopscience.iop.org/0953-8984/17/6/011)

INSTITUTE OF PHYSICS PUBLISHING JOURNAL OF PHYSICS: CONDENSED MATTER

J. Phys.: Condens. Matter **17** (2005) 923–948 doi:10.1088/0953-8984/17/6/011

# Photoluminescence and reversible photo-induced spectral change of $SrTiO_3$

**Shosuke Mochizuki**[1], **Fumito Fujishiro and Seiko Minami**

Department of Physics, College of Humanities and Sciences, Nihon University, 3-25-40 Sakurajosui, Setagaya-ku, Tokyo 156-8550, Japan

E-mail: motizuki@physics.chs.nihon-u.ac.jp

Received 7 June 2004, in final form 4 January 2005
Published 28 January 2005
Online at stacks.iop.org/JPhysCM/17/923

**Abstract**

When strontium titanate ($SrTiO_3$) single crystal is irradiated at room temperature with a 325 nm laser light in an evacuated specimen chamber, the luminescence intensity increases, creating a broad visible luminescence centred at about 2.4 eV. Then, introducing oxygen gas into the specimen chamber, the photoluminescence spectrum returns reversibly to the original weak luminescence under the same laser light irradiation. After removing the laser light irradiation, each photoluminescent state is stored for a long time at room temperature under room light, regardless of any changes of atmosphere. Such photo-induced spectral change has been observed also at different temperatures from 13 K to room temperature. The observed phenomenon is explained by means of the photo-induced oxygen defect formation at the surfaces of $SrTiO_3$ crystal. For the same $SrTiO_3$ single crystal, we have studied the photoluminescence properties. Besides the 2.4 eV luminescence band, we have observed new two luminescence bands centred at about 3.2 eV and about 2.9 eV. The energy, 3.2 eV, is close to both the photoluminescence excitation edge energy and the reported band edge energy of $SrTiO_3$ crystal. Both the 3.2 eV luminescence and the 2.9 eV luminescence decay rapidly after a pulsed photoexcitation, while the 2.4 eV luminescence lasts for several seconds at 13 K. The excitation light intensity dependence of these luminescence bands has been also measured at 13 K. The 2.4 eV luminescence increases in intensity with increasing excitation intensity up to 4 mJ $cm^{-2}$, and then it becomes decreased with further increase in the excitation intensity. On the other hand, both the 3.2 eV luminescence and the 2.9 eV luminescence increase in intensity with increasing excitation intensity, without any saturation. Although the 2.4 eV luminescence had been assigned to the radiative decay of intrinsic self-trapped excitons in a superparaelectric state by several workers, the present studies have clarified that the luminescence originates mainly from crystal defects (oxygen defects and chemical heterogeneity in the surface region).

[1] Author to whom any correspondence should be addressed.

  

Both the 3.2 eV luminescence and the 2.9 eV luminescence are discussed qualitatively.

## 1. Introduction

Considerable attention has been given to clarifying the quantum paraelectric state in strontium titanate ($SrTiO_3$). The lattice of $SrTiO_3$ has the cubic perovskite-type structure at room temperature. At 105 K, it transforms into a tetragonal structure. With temperature decreasing from room temperature, the static dielectric constant increases prominently, and it attains several ten thousands at 4 K without any paraelectric–ferroelectric transition (Müller and Burkard 1979). Between 4 and 0.3 K, the dielectric constant was found to be independent of temperature. Recently, a prominent enhancement of the dielectric constant has been observed under ultraviolet light irradiation (Katsu *et al* 2001, Takesada *et al* 2003, Hasegawa *et al* 2003), but it is now under dispute, involving some complicated problems relating to electrode/$SrTiO_3$ interfaces. In order to explain the quantum paraelectric state, one may assume first that $Ti^{4+}$ ions are fluctuating quantum mechanically in the $SrTiO_3$ lattice, as if they are in the critical state just before the paraelectric–ferroelectric transition in usual ferroelectrics. Müller *et al* (1991) proposed that $SrTiO_3$ is in a coherent quantum state associated with a rotonic minimum in the transverse acoustic mode. For the photo-enhanced dielectric constant, Nasu (2004) assumed that ultraviolet light broke the crystal inversion symmetry, creating ferroelectric microdomains. He assumed also that such microdomains fluctuated and itinerated quantum mechanically in the $SrTiO_3$ crystal. $SrTiO_3$ crystal has an indirect gap and a direct gap in an energy range between about 3.2 eV and about 3.5 eV (Cohen and Blunt 1968, Blazey 1971, Capizzi and Frova 1970, Capizzi *et al* 1972, Cardona 1965, Zollner *et al* 2000, Hasegawa *et al* 2000). It is known that the luminescence intensity is specimen dependent (Grabner 1969). Hasegawa *et al* (2000) measured the optical absorption and photoluminescence spectra at temperatures between 10 K and room temperature. They found that the crystal exhibited a broad photoluminescence band around 2.4 eV. Through time-resolved photoluminescence measurements, they assigned the 2.4 eV luminescence to the radiative decay of intrinsic self-trapped excitons. However, many metal oxides display very similar broad photoluminescence between 2 and 3 eV: for example, $Sm_2O_3$ (Mochizuki 2003), $Eu_2O_3$ (Mochizuki *et al* 2001), anatase $TiO_2$ (Mochizuki *et al* 2003), $Al_2O_3$ (Mochizuki and Araki 2003a), vitreous $SiO_2$ (Mochizuki and Araki 2003b) and $LaAl_2O_3$ (Kawabe *et al* 2000). Moreover, their luminescence intensities are specimen dependent, especially as regards the thermal history and crystal preparation method. Unfortunately, this specimen-dependent nature of the 2.4 eV luminescence has been accorded too little respect in the optical study of $SrTiO_3$ and it has led many researchers astray.

Very recently, we have found at room temperature that the 2.4 eV luminescence band of $SrTiO_3$ grows under a 325 nm laser light irradiation in vacuum, while it disappears under the same laser light irradiation in oxygen gas. Through many successive experiments involving replacing the specimen atmosphere, it was found that the spectral change occurs reversibly under the 325 nm laser light irradiation. The observed phenomenon relates to the photo-induced oxygen defects at the surfaces of $SrTiO_3$. Now or never is the time to reinvestigate the photoluminescence properties of $SrTiO_3$ in detail, taking account of such oxygen defects.

In the present paper, we report the photoluminescence spectrum, its excitation intensity dependence, the decay profile, the photoluminescence excitation spectrum, the time-resolved photoluminescence spectrum and the reversible photo-induced spectral change of $SrTiO_3$ single crystal at different temperatures between 12 K and room temperature in detail.

## 2. Experimental detail

The $SrTiO_3$ crystal was well grown by the Verneuil method and the as-grown crystal is dark blue. The as-grown crystal was then annealed under an appropriate reducing atmosphere. The crystal became perfectly colourless and transparent under the annealing. Several as-grown (dark blue) and annealed (colourless transparent) $SrTiO_3$ single crystals, $10 \times 10 \times (0.5–1.0)$ mm in size, were supplied by Sinkosya Corporation. The broad surfaces of the crystals are optically flat and they are oriented in the [100] direction. It should be noted that such transparent $SrTiO_3$ crystals grown by the Verneuil method have been widely used by many workers for studying electrical and optical properties. As reference specimens, we have used also several $SrTiO_3$ powder compact discs which were sintered at 1273 K and annealed at different atmosphere.

The photoluminescence (PL) spectra were measured by using an optical multichannel analyser consisting of a grating monochromator (focal length = 32 cm, grating = 1200 or 150 grooves $mm^{-1}$) and an image-intensified diode-array detector (number of channels = 1024, gate time = 5 ns). An $Nd^{3+}$:YAG laser (wavelength = 355 nm, pulse width = 4–5 ns, repetition = 10 Hz), a continuous wave (CW) He–Cd laser (wavelength = 325 nm) and a monochromatic light source consisting of a 150 W xenon lamp and a grating monochromator (focal length = 20 cm) were used as the excitation source. The excitation light intensity dependence of the PL spectrum was measured by attenuating the incident laser light intensity with glass attenuators calibrated in transmissivity. The PL excitation (PLE) spectra were recorded by varying the excitation light wavelength $\lambda_{ex}$ with the same monochromatic light source as described above, and by detecting the luminescence light intensity at a desired wavelength $\lambda_{ob}$ as a function of $\lambda_{ex}$ with a grating monochromator (focal length = 20 cm) and a synchronous light detection system. The time-resolved PL spectra were taken using the same optical multichannel analyser to which two delay pulse generators were attached. The delay time $t_d$, which is the measurement start time after a laser pulse incidence, and the gate time $t_g$, which is the time after $t_d$ of the spectral measurement, were set with these delay pulse generators which were controlled with a personal computer. The actual minimum gate time was 5 ns. The decay curves were measured with an apparatus consisting of a grating monochromator (focal length = 20 cm) equipped with a photodetection system (time constant = about 1 $\mu$s) and the $Nd^{3+}$:YAG laser oscillating at 355 nm. The optical density (OD) spectrum was measured using another optical multichannel analyser.

An optical cryostat was used for the specimen chamber, in which a closed-cycle helium refrigerator equipped with a temperature controller was used to change the specimen temperature between 12 K and room temperature. Another specimen chamber was also used for the measurement of the reversible spectral change at room temperature. An oil-free vacuum system was used for evacuating these specimen chambers.

## 3. Results

### *3.1. Photoluminescence spectra of $SrTiO_3$ under weak excitation*

Figure 1(a) shows the PL spectra of $SrTiO_3$ at different temperatures under a pulsed 355 nm laser light excitation (pulse width = 4–5 ns, repetition = 10 Hz, fluence = 0.079 mJ $cm^{-2}$). A broad luminescence band is observed around 2.4 eV at 12 K. The band seems slightly asymmetrical in spectral shape and it consists of two luminescence bands centred at 2.46 and 2.40 eV, which are labelled B′ and B″, respectively. This indicates that this photoluminescence comes from at least two kinds of luminescent centres. The spectral shape and intensity differ slightly with the specimens. We measured also the PL spectra of an as-grown crystal as a function of annealing time at 973 K in a reducing atmosphere. It has been found that the PL

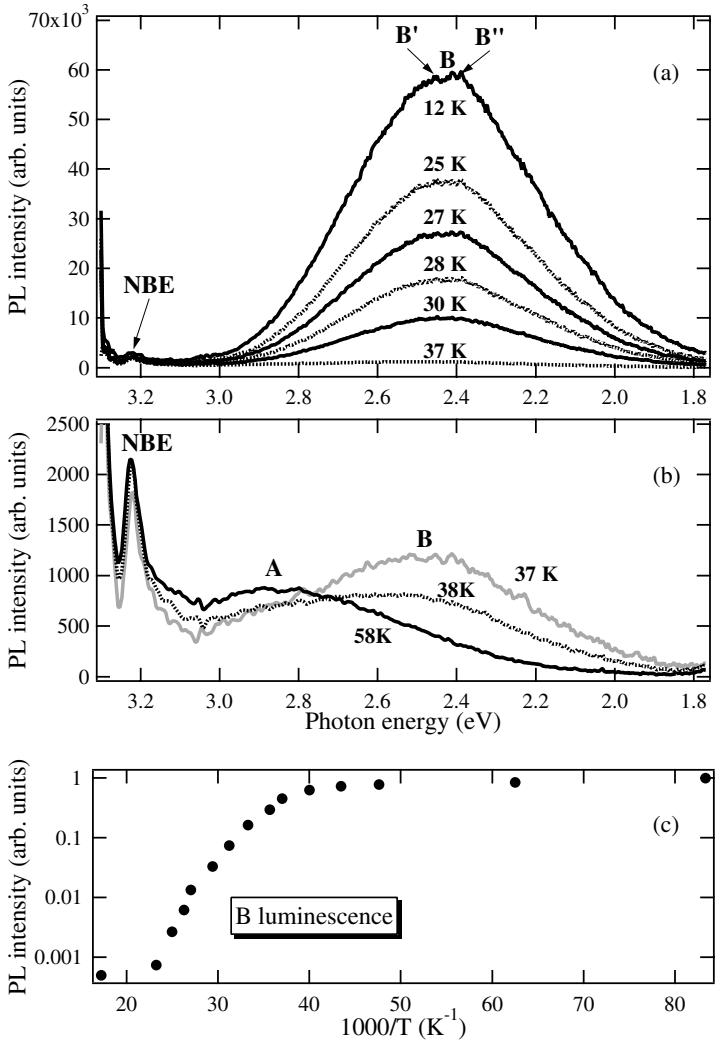


**Figure 1.** The photoluminescence spectra of $SrTiO_3$ at different temperatures: (a) $T \leqslant 37$ K; (b) $T \geqslant 37$ K. (c) The temperature dependence of the integrated intensity. The excitation laser fluence was 0.079 mJ cm$^{-2}$. The spectral integration was performed in a photon energy range between 2.9 and 1.77 eV.

intensity increases with increasing annealing time, while the PL intensity peak energy and spectral width are slightly dependent on the annealing time. With increasing temperature, the 2.46 eV luminescence band grows more and then this band becomes together with the 2.40 eV luminescence band, displaying an asymmetrical band centred at about 2.44 eV above 27 K. We call this luminescence band the 'B luminescence band'. On further increasing the temperature, the B luminescence intensity continues to decrease, while a new luminescence band appears at 2.89 eV and becomes prominent, as seen in figure 1(b). We tentatively call this luminescence band the 'A luminescence band'. The A luminescence band seems to extend above 3.2 eV. The A luminescence band grows to the detriment of the B luminescence and it is superior to the B luminescence band above 58 K. The integrated PL intensity of the B luminescence band is plotted against inverse temperature on a semi-logarithmic scale in figure 1(c). The

spectral integration was performed in a photon energy region between 2.9 and 1.77 eV. In this figure, the maximum luminescence intensity is normalized to unity. As seen in this figure, the luminescence intensity decreases gradually with increasing temperature to 25 K and, on further increasing the temperature above 28 K, the intensity decreases exponentially. Approaching 43 K, the intensity becomes constant. Although such temperature dependence approaching a constant has been not reported for $SrTiO_3$, a slight sign of such constant intensity appeared in the reported curve (figure 3(b): Hasegawa *et al* 2000), as some deviation from the curve fitting to the data. The constant intensity is due to the A luminescence component which grows gradually at high temperatures. Although the PL band consists of several luminescence components as described above, we subtract the constant intensity from the data and we assume a phonon-assisted non-radiative decay process for the observed B luminescence. Then, we perform a curve fitting by using the well-known expression for the integrated PL intensity $I(T)$,

$$I(T) = \frac{1}{1 + C\exp(-\Delta E/kT)}, \tag{1}$$

where $C$ is a constant and $\Delta E$ is the height of an average potential barrier separating a luminescent state from the ground state. In addition to such a phonon-assisted non-radiative process, thermal ionization of luminescence states is also considered to participate in the intensity decrease with increasing temperature. In such a case, $\Delta E$ may correspond to the ionization energy. In the fitting, the data obtained above 40 K are taken off to avoid the effect of the A luminescence. The best-fitted curve is obtained with a $\Delta E = 32$ meV. The value is slightly smaller than the value (43 meV) reported by Hasegawa *et al* (2000). At present, it is not clear whether the difference arises from the specimen-dependent nature or from the error in the specimen surface temperature measurements or from the manner of the curve fitting—performed probably ignoring the effect of the A luminescence.

As seen in figures 1(a) and (b), a sharp luminescence band is also observed at 3.23 eV which is close to the observed PLE edge (3.26 eV) and the reported indirect band gap energy $E_g^{id}$ (3.27 eV) of $SrTiO_3$. We tentatively call this luminescence band appearing near the band edge the 'NBE luminescence band'. The steep rise above 3.26 eV is due to the parasitic luminescence of the optical multichannel analyser used.

### *3.2. Photoluminescence excitation spectra of $SrTiO_3$*

The photoluminescence excitation (PLE) spectra of the same $SrTiO_3$ single crystal have also been measured at different temperatures. Some of the spectra are selected and shown in figure 2, in which the PL spectrum observed at 13 K is also shown. The luminescence intensity was monitored at the intensity peak energy of the B luminescence band. The PLE spectrum displays a sharp edge at 3.26 eV and a kink at 3.42 eV, which are close to the reported indirect gap energy $E_g^{id}$ (3.27 eV) and the direct gap energy $E_g^{d}$ (3.46 eV) of $SrTiO_3$ (Capizzi and Frova 1970), respectively. The PLE spectrum indicates that the B luminescence is caused mainly by the interband excitations. The energy difference of the B luminescence band from the PLE edge is about 0.80 eV. The shape of the PLE spectrum differs in an energy region higher than the PLE edge from the absorption spectra reported by Blazey (1971), Capizzi and Frova (1970), Capizzi *et al* (1972), Cardona (1965) and Zollner *et al* (2000). Generally, there are many crystal defects at the specimen surfaces where photoexcited states tend to decay non-radiatively. Such a luminescence quench effect appears more prominently in an energy region higher than the fundamental absorption edge. The excitation with photons above the band gap energy produces energetic electrons and holes, which are eventually thermalized by emitting phonons. Therefore, the PLE above the band gap is governed not necessarily by the direct

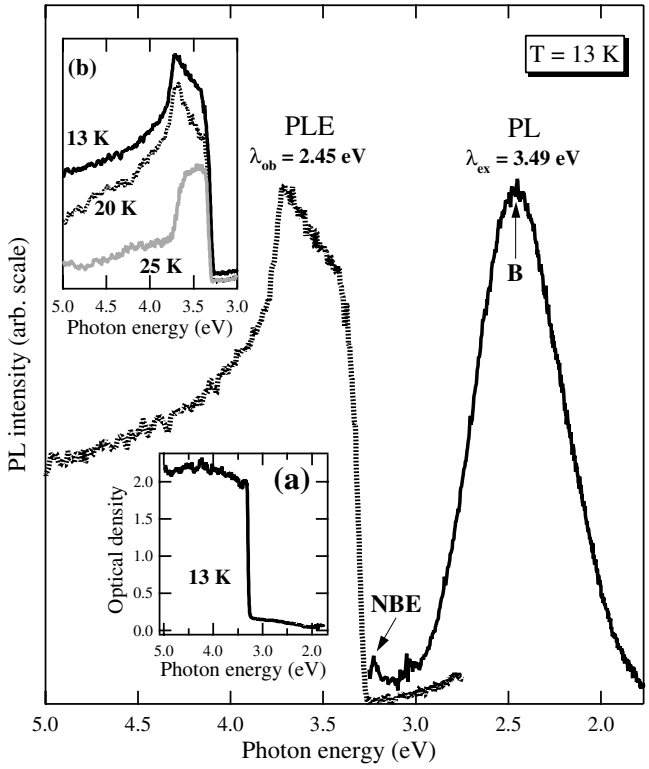


**Figure 2.** The photoluminescence (PL), optical density (OD) and photoluminescence excitation (PLE) spectra of $SrTiO_3$ at 13 K. The luminescence is monitored at the peak energy (=2.45 eV) of the B luminescence band. The OD spectrum at 13 K and the PLE spectra at different temperatures are shown in inset (a) and inset (b), respectively.

quenching of highly excited electrons at defect sites but by the change in the probability of the interaction of electron–hole pairs with defects.

As shown in inset (a) of figure 2, the OD spectrum has a faint tail below 3.2 eV. It is found that the OD of the tail decreases with annealing in a reducing atmosphere. Although the B luminescence band is well excited by the interband transition, the PLE spectra indicate that the luminescence can also be excited even by photons having energies lower than indirect gap. Under a 442 nm (=2.80 eV) laser light excitation, we have certainly detected the B luminescence spectrum through a laser light sharp cut filter (HOYA: Y48). The B luminescence can also be ascertained clearly by the naked eye through the same filter. Under the same 442 nm excitation, we have also found more intense luminescence for sintered $SrTiO_3$ powder compact specimens (Mochizuki and Fujishiro 2005). These results indicate that there are different defect-related luminescent levels in the energy gap.

As seen in inset (b), the PLE spectral shape changes with increasing temperature, except for the absorption edge profile. The suppression seen at photon energies higher than 3.7 eV becomes prominent with increasing temperature. The suppression may arise from the temperature change in the probability of the interaction of electron–hole pairs with defects.

In the following sections, the observed energy difference (0.8 eV), together with the photo-induced spectral change, will be discussed, and it will be concluded that the B luminescence band comes from the extrinsic luminescent centres around which photo-generated carriers (free electron or free hole, or both) are trapped.

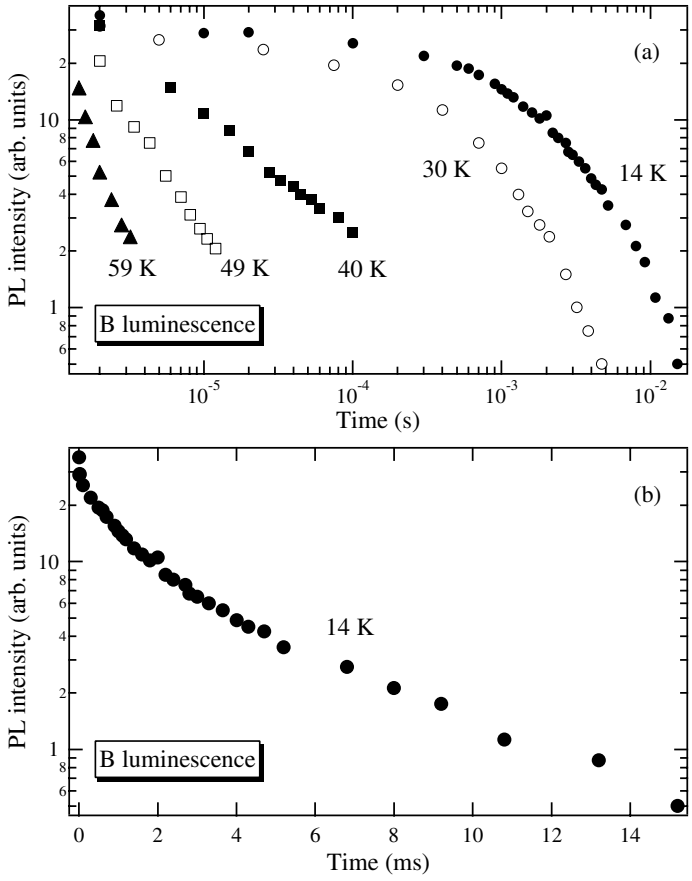


**Figure 3.** The photoluminescence decay profile of the B luminescence band of $SrTiO_3$: (a) log (PL intensity)–log $t$ plots at different temperatures, (b) log (PL intensity)–$t$ plots at 14 K. The photoluminescence was monitored at 2.45 eV. The 355 nm excitation laser fluence was approximately 0.2 mJ $cm^{-2}$.

### *3.3. The photoluminescence decay profile of $SrTiO_3$*

We have measured the luminescence decay curves of the B luminescence of the same $SrTiO_3$ single crystal at different temperatures. The luminescence was monitored at an intensity peak wavelength of the B luminescence band. Figure 3(a) shows the PL decay profiles of the B luminescence at different temperatures. The PL intensity is plotted against time on a log–log scale. The decay profile at 14 K is also displayed as a semi-log plot in figure 3(b). It is noted that the crystal displays luminescence for times longer than several tens of milliseconds at 14 K. The profile at 14 K can be well expressed as a three-component exponential decay curve,

$$I(t) = I_1 \exp(-t/\tau_1) + I_2 \exp(-t/\tau_2) + I_3 \exp(-t/\tau_3), \tag{2}$$

with the following parameters:

$I_1 = 15.408$, $\tau_1 = 2.6533 \times 10^{-6}$ s, $I_2 = 11.134$, $\tau_2 = 5.4218 \times 10^{-4}$ s,
$I_3 = 16.909$, $\tau_3 = 2.8396 \times 10^{-3}$ s.

Since the photodetection system used for decay curve measurements has a long time constant (about 1 $\mu$s), the shorter lifetime component is not resolved. Therefore, the B luminescence may arise from at least three kinds of luminescence centres.

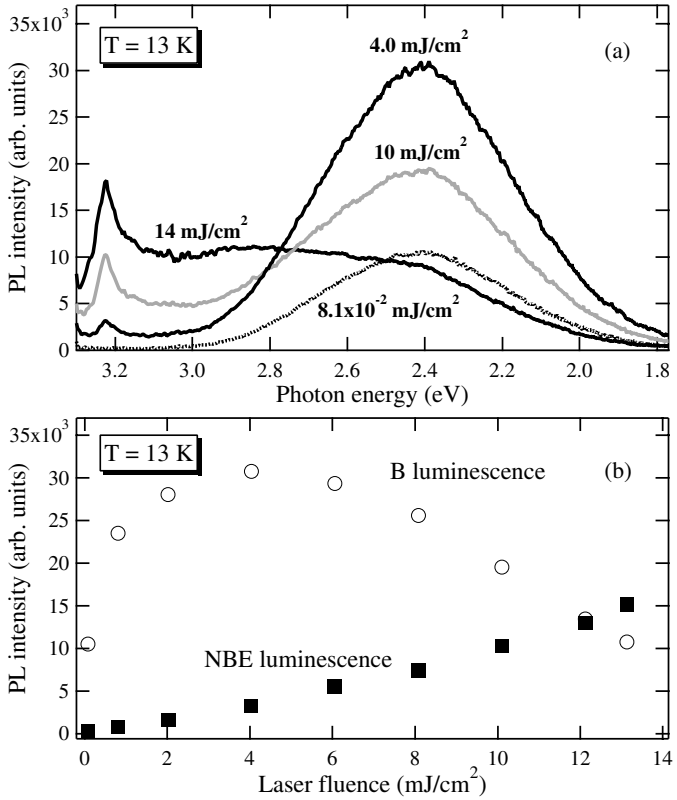


**Figure 4.** The excitation light intensity dependence of the photoluminescence spectrum of $SrTiO_3$ at 13 K: (a) spectra under intense, medium and weak excitations; (b) the excitation laser fluence dependence of the peak intensities of the near-band-edge luminescence (NBE) band and the B luminescence band. The NBE luminescence peak energy and the B luminescence peak energy are 3.2 and 2.4 eV, respectively.

Alternatively, the same decay data were examined with a power law ($t^{-n}$). It is found that the curve cannot be uniquely expressed with the $t^{-2}$ law (Tsang and Street 1979); rather it has a $t^{-1-2}$ dependence. Hasegawa *et al* (2000) performed also decay curve fitting with the $t^{-n}$ law, and they inferred suitability of the $t^{-2}$ law for $SrTiO_3$. However, a caution should be required for result to differ greatly by which data points are selected for the curve fitting with the power law.

At the present stage, the observed decay curve should be regarded obediently as an exponential decay curve consisting of different components. The long lifetime component may arise from some radiative transitions of different deeply trapped states. After stopping the laser irradiation of the as-grown and annealed $SrTiO_3$ crystals, we frequently observed faint phosphorescence lasting for several seconds, with the naked eye. Unfortunately, the decay time of such a phosphorescence component ($t \gg 10^{-3}$ s) cannot be determined from the decay curve analysis, because the phosphorescence contribution to the decay curve is too small.

### *3.4. Photoluminescence spectra of $SrTiO_3$ under intense excitation*

We have measured the PL spectra of the same $SrTiO_3$ single crystal at different excitation laser fluences. A typical result is shown in figure 4(a). In figure 4(b), the peak intensities of the

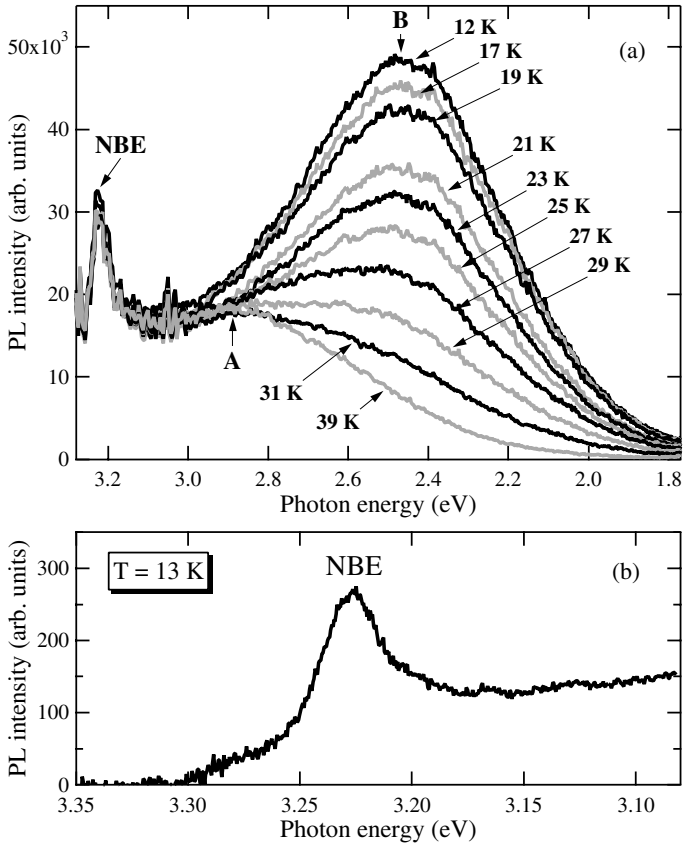


**Figure 5.** The photoluminescence of $SrTiO_3$ under intense photoexcitation: (a) photoluminescence spectra at different temperatures ($T \leqslant 39$ K). The 355 nm excitation laser fluence was 0.93 mJ cm$^{-2}$. (b) Near-band-edge (NBE) emission at 13 K. The 355 nm excitation laser fluence was 12 mJ cm$^{-2}$.

NBE and the B luminescence bands are plotted against laser fluence. Solid squares and hollow circles correspond to the NBE luminescence and the B luminescence, respectively. Under weak excitation, only a B luminescence band is observed. With increasing laser fluence, the B luminescence intensity increases monotonically, and the NBE and A luminescence bands appear. On the laser fluence further increasing up to 4 mJ cm$^{-2}$, the B luminescence attains a maximum, while both the NBE luminescence and the A luminescence become prominent. On laser fluence exceeding 4 mJ cm$^{-2}$, the B luminescence intensity begins to decrease monotonically, while both the NBE luminescence band and the A luminescence band continue to grow, degrading the B luminescence band. Incidentally, we have found that the B luminescence intensity maximum appeared at 0.4 mJ cm$^{-2}$ for the sintered $SrTiO_3$ powder compact. This suggests that most of the B luminescence centres are at the specimen surface.

In order to study the NBE, A and B luminescence bands in detail, we have measured the PL spectra at different temperatures under an intense excitation of 0.93 mJ cm$^{-2}$. This excitation intensity is enough to show up all of the luminescence bands. The results are shown in figures 5(a), 6(a) and (b). We subtract the spectrum measured at 297 K from the spectrum measured at 12 K, in an attempt to extract the B luminescence component. The difference spectrum is given in figure 6(c). By comparing this spectrum with the spectrum (figure 1(a)) observed at the same temperature under a weak photoexcitation, it was found that the spectral

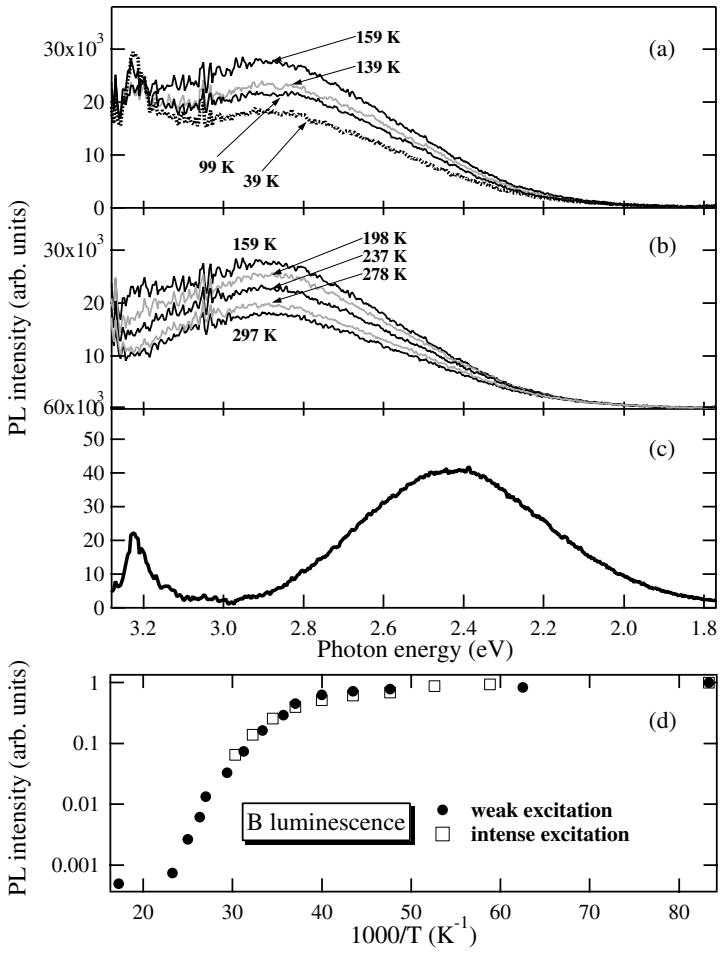


**Figure 6.** The photoluminescence of $SrTiO_3$ under intense photoexcitation (0.93 mJ $cm^{-2}$): (a) photoluminescence spectra at different temperatures (39 K $\leqslant T \leqslant$ 159 K); (b) photoluminescence spectra at different temperatures (159 K $\leqslant T \leqslant$ 297 K); (c) the difference spectrum; (d) the temperature dependence of the integrated intensity of the B luminescence band for weak and intense excitations which were 0.079 and 0.93 mJ $cm^{-2}$, respectively. The spectral integration was performed in a photon region between 2.9 and 1.77 eV.

shape of the B luminescence band is almost independent of the photoexcitation intensity. With temperature increasing up to 39 K, the B luminescence intensity decreases and then it disappears at 39 K, while the NBE and A luminescence intensities are almost constant. With temperature increasing above 39 K, the A luminescence band continues to grow more without changing the spectral shape and then it attains a maximum at 159 K, while the NBE luminescence band becomes weak with the spectral broadening and is merged in the A luminescence band at 198 K. At present, it is not clear why such a phonon-assisted nature of the A luminescence band arose. With the temperature further increasing above 159 K, the A luminescence intensity decreases. This intensity decrease may be due to non-radiative traps. The PL spectrum measured at 297 K was subtracted from that measured at different temperatures, and then the spectral integration was performed over a photon energy range between 2.9 and 1.77 eV. The integrated intensities thus obtained for the B luminescence band are plotted against inverse temperature, as hollow

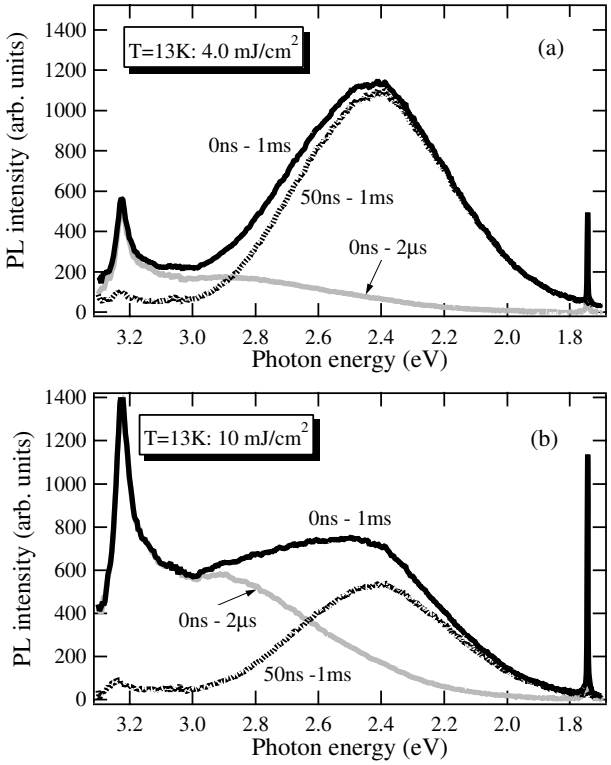


**Figure 7.** The time-resolved photoluminescence spectra of $SrTiO_3$ at 13 K: (a) laser fluence = 4.0 mJ $cm^{-2}$; (b) laser fluence = 10 mJ $cm^{-2}$.

squares, in figure 6(d). The data obtained for weak excitation, which are already shown in figure 1(c), are also plotted as solid circles in this figure.

Under a high laser fluence (12 mJ $cm^{-2}$), more detailed measurements were performed also on the NBE luminescence and the A luminescence, using a high resolution monochromator. This laser fluence is enough to show up the NBE and A luminescence bands. The result obtained at 13 K is given in figure 5(b). As seen in this figure, the NBE luminescence band is on the rise of the A luminescence band. The NBE luminescence peak is about 77 meV lower in energy than the onset energy of the A band, and it is about 34 meV lower than the PLE edge energy. The NBE luminescence band and the A luminescence have similar temperature and excitation intensity dependences. This suggests that the NBE luminescence and the A luminescence have the same origin.

Most of luminescent metal oxides show some photo-darkening effects under intense photoexcitation. It is found that the PL spectrum and PL intensity of the $SrTiO_3$ single crystal used were almost unchanged, in spite of such intense 355 nm photoexcitation (14 mJ $cm^{-2}$).

### *3.5. Time-resolved photoluminescence spectra of $SrTiO_3$*

Time-resolved photoluminescence spectra of the same $SrTiO_3$ single crystal have been measured at 13 K under different excitation intensities. To study the time evolutions of all of the luminescence bands, the measurements were performed under intense excitation. The spectra obtained under excitations of 4.0 and 10 mJ $cm^{-2}$ are shown in figures 7(a) and (b), respectively. The measurement times, $t_d$ and $t_g$, are given by each curve. At the

initial stage of photoexcitation, the laser light pulse is seen at twice the wavelength, 710 nm (=355 nm × 2 = 1.745 eV), of each spectrum, which is common to every grating monochromator. Both the NBE luminescence and the A luminescence disappear rapidly within 50 ns after excitation. Taking account of the parasitic delay, timing jitter times of the apparatus used and the actual laser pulse duration ($\leqslant$10 ns), the lifetimes of the NBE and A luminescences are estimated to be less than 10 ns. The B luminescence band is growing over time between 50 ns and 1 ms, and the spectral shape is almost unchanged with further increase in time. The B luminescence observed between 50 ns and 1 ms is slightly shifted toward the lower energy side of the B luminescence observed between 0 ns and 1 ms, as shown in figure 7(a). The shift is due to the time integration effect on the PL intensity. The measured intensity between $t_d$ and $t_g$ is expressed as follows:

$$I(t) = \sum_j \int_{t_d}^{t_g} \eta_j N_j(t=0) \mathrm{e}^{-t/\tau_j}\, \mathrm{d}t, \tag{3}$$

where $\eta_j$, $N_j(t=0)$ and $\tau_j$ are the quantum yield, number and lifetime of $j$th luminescence centre including the extrinsic and intrinsic luminescence centres, respectively. If the luminescence centres responsible for the B luminescence band differ slightly in energy, a small shift may be anticipated, as is in fact observed.

Both the PLE spectrum shown in figure 2 and these time-resolved spectra show clearly that the B luminescence follows the NBE and A luminescence. The long lifetime luminescence, continuing for more than several tens of milliseconds, like the B luminescence, is not peculiar to $SrTiO_3$ but such long lasting luminescence is frequently observed for different metal oxides, for example, $ZrO_2$ (Fujishiro and Mochizuki 2005). This indicates that the B luminescence cannot necessarily be connected with the nature of the quantum paraelectric state. Such long lifetime luminescence observed for different oxides is thought to arise from accidental recombination of shallowly trapped electrons with distant holes localized around defects. In such a case, the luminescence has slightly different long lifetimes, as seen in figures 3(a) and (b), and the B luminescence spectral shape is almost unchanged with time, as seen in figures 7(a) and (b).

### *3.6. Reversible photo-induced spectral change in $SrTiO_3$*

When the same $SrTiO_3$ single crystal is irradiated with a CW 325 nm laser light at room temperature in an evacuated chamber, the B luminescence intensity is enhanced to about twice. Then, introducing oxygen gas into the specimen chamber, the intense PL state returns to the original weak one under the same laser light irradiation, with increasing irradiation time. Through many successive experiments, it was found that the spectral change is nearly reversible under 325 nm laser light irradiation. After removing the 325 nm laser light irradiation, each PL state is stored for a long time at room temperature under room light, regardless of any changes of atmosphere. A typical example of the photo-induced spectral change obtained is shown in figure 8. The experiments were carried out in the following order: (a) → (b) → (c) → (d). Irradiation times $t_{ir}$ under a given atmosphere and the kind of atmosphere are indicated by each curve. Irradiating under oxygen gas considerably decreases the PL intensity of the specimens. In figure 9, the difference spectrum, curve 7 − curve 8, is shown. The PL spectral change observed for the $SrTiO_3$ single crystal is mainly characterized by an intensity change of the B luminescence band. A slight degradation of the PL intensity is observed, which may be caused by some photo-induced non-radiative centres. The same experiments were carried out by changing the wavelength of the irradiating laser light. No spectral change was observed except for the CW 325 nm laser light. It was found that the speed of the change accelerates on increasing the power density of the activating light.

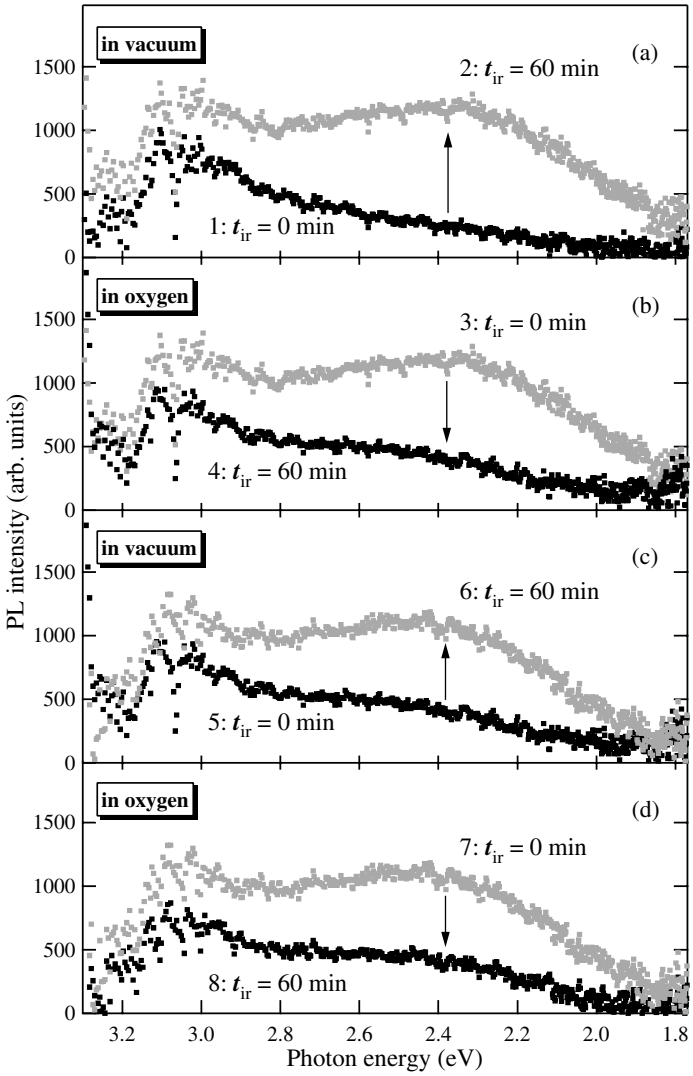


**Figure 8.** The photo-induced reversible spectral change of $SrTiO_3$ at room temperature: (a) in vacuum, (b) in oxygen gas, (c) in vacuum, (d) in oxygen gas. The experiments were carried out in the following order: (a) → (b) → (c) → (d). Each irradiation was carried out for 60 min under a given atmosphere. Each spectral change is indicated by an arrow. The 325 nm laser fluence was 0.79 W $cm^{-2}$.

Similar photo-induced spectral change has been observed at different temperatures from 13 K to room temperature. The result obtained at 13 K in vacuum under irradiation with 325 nm laser light is shown in figure 10(a), as a typical result. The $t_{ir}$ in vacuum is indicated by each curve. The peak intensity is plotted against $t_{ir}$ in figure 10(b). With increasing $t_{ir}$, the intensity increases and then tends to saturate at 90 min. The intensity increase is proportional to $t_{ir}^n$ ($n < 1$). It has been found that the magnitude of the spectral change for 60 min is nearly independent of temperature. After stopping the laser light irradiation, the photoluminescence intensity decreases slightly with increasing time and then reaches a steady state value, which is a photomemory phenomenon.

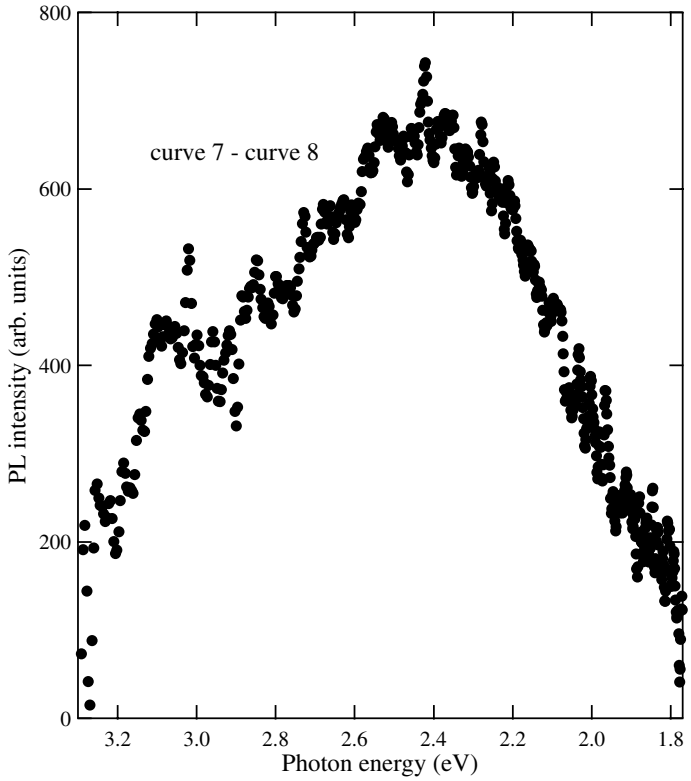


**Figure 9.** The difference spectrum for curve 7 and curve 8. Curves 7 and 8 are shown in figure 8.

Like for $Sm_2O_3$ (Mochizuki 2003), $Eu_2O_3$ (Mochizuki *et al* 2001), anatase $TiO_2$ (Mochizuki *et al* 2003) and vitreous $SiO_2$ (Mochizuki and Araki 2003b), the observed spectral transition may arise from photo-induced oxidation and photo-induced reduction.

### *3.7. Photoluminescence properties of as-grown $SrTiO_3$*

In order to elucidate the crystal defect effects on the photoluminescence more directly, we have studied the reversible photo-induced spectral transition for an as-grown Verneuil $SrTiO_3$ crystal at room temperature. The as-grown $SrTiO_3$ crystal is dark blue. The luminescence was excited also with a 325 nm laser line of the He–Cd laser. The result is shown in figure 11(a). Curve 1 is the spectrum of the as-grown crystal. The PL intensity of the as-grown crystal is stronger than several thousands times that of the annealed crystal. The spectrum consists of at least three luminescence bands, at 2.9, 2.3 and 2.2 eV. Curve 2 is the spectrum measured after irradiating in oxygen gas for 60 min. Under 325 nm laser light irradiation in oxygen gas, the PL intensity is decreased considerably. The degradations of the 2.3 and 2.2 eV luminescence bands are especially prominent. The specimen chamber is evacuated again. Curve 3 and curve 4 are the spectra measured at 60 and 480 min after beginning irradiation in vacuum, respectively. Then, oxygen gas was introduced again into the specimen chamber. Curve 5 is the spectrum measured at 840 min after beginning irradiation in oxygen gas. The integrated PL intensity of curve 4 is increased more than 16 times compared with that of curve 5. In figure 11(b), curve 4 is compared after rescaling curve 5 so as to fit to curve 4 at photon energies higher than 2.8 eV. The rescaled curve is shown as curve 5′. Like for the annealed transparent

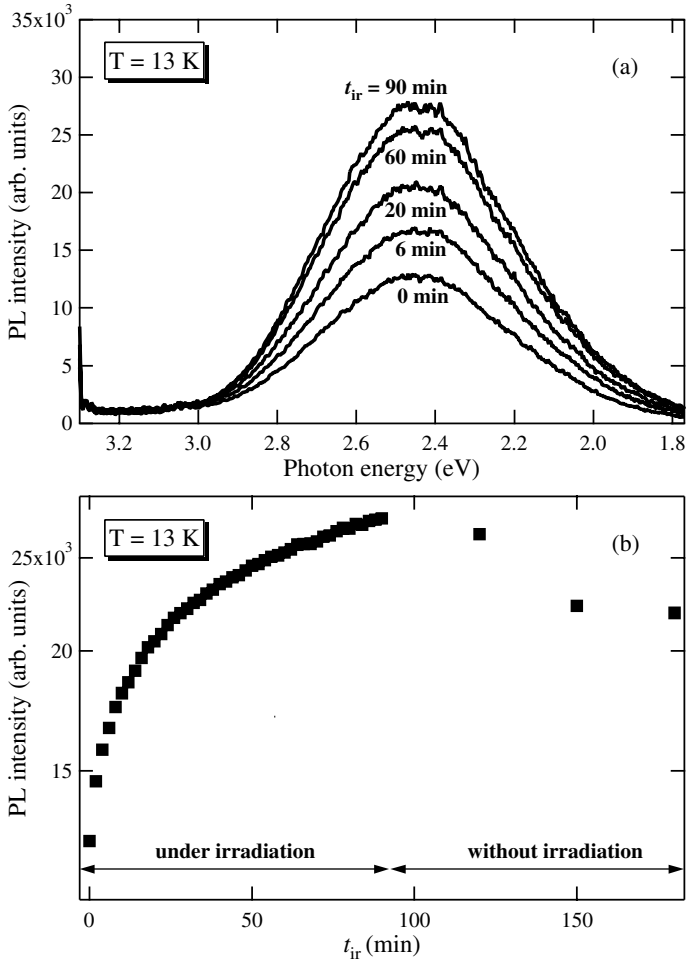


**Figure 10.** The photo-induced spectral change of $SrTiO_3$ at 13 K in vacuum: (a) photoluminescence spectra for 325 nm laser light irradiation; the irradiation time is indicated by each curve; (b) the irradiation time dependence of the peak intensity of the photoluminescence. The 325 nm laser fluence was 0.79 W $cm^{-2}$.

$SrTiO_3$ crystal, an A-like luminescence appears in the as-grown crystal: compare curve 5 in figure 11(a) with curve 8 in figure 8(d) and the curve observed at 297 K in figure 6(b). To deduce the information on the B luminescence observed in the annealed $SrTiO_3$ crystal, the difference spectrum (curve 4 − curve 5′) was calculated; it is shown in figure 11(b). We can find a broad luminescence band centred at 2.3 eV, which is slightly shifted to the lower energy side of the B luminescence band of the annealed crystal. It is noted that the B luminescence intensity for the as-grown and the annealed crystals can be varied by 325 nm laser light irradiation in vacuum and in oxygen gas. Since the light penetration depth is very small at 325 nm for $SrTiO_3$ (Zollner *et al* 2000), the observed spectral change of the B luminescence band could be closely related to the change of surface electronic states.

Using the same as-grown crystal, we have measured the photoluminescence spectra at different temperatures under an intense excitation (14 mJ $cm^{-2}$). As a typical result, the spectrum obtained at 12 K is shown in figure 12. The spectrum obtained at 13 K under the

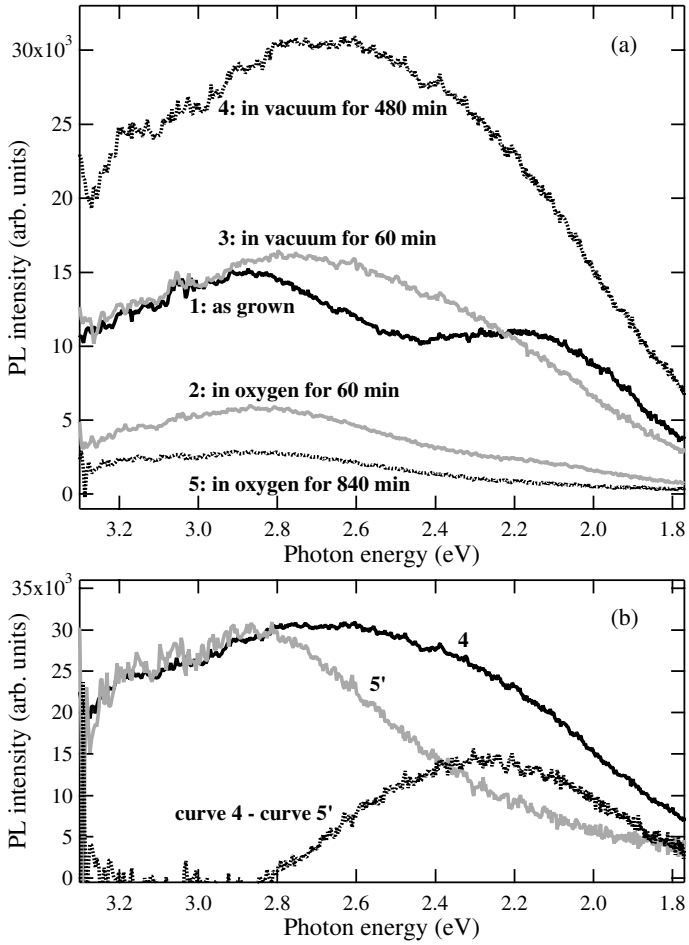


**Figure 11.** The photo-induced reversible spectral change of as-grown $SrTiO_3$ at room temperature: (a) photo-induced spectral change for replacing specimen atmosphere, (b) comparison of curve 4 with curve 5. The 325 nm laser fluence was 0.79 W $cm^{-2}$.

same excitation intensity for the annealed crystal is also shown; this was already shown in figure 4(a). The NBE and A luminescence are considerably enhanced in the as-grown crystal. The fine structure and PL intensity of the NBE luminescence band depend on the annealing time. The results suggest that the NBE and A luminescence are assisted by crystal defects.

### *3.8. Miscellaneous*

We have measured the PL spectra of sintered $SrTiO_3$ powder compacts at different temperatures and different laser fluences. The powder specimens show clearly the NBE, A and B luminescences. The NBE and A luminescences remain at room temperature, while the B luminescence disappears above 40 K. Most of the PL properties were very similar to those of single-crystal specimens. Like for other luminescent oxides, the powder compacts were less luminescent and their luminescence decay lifetimes were shorter than those of the single crystals. The main difference between the cases for the powder compacts and the single crystals is that the B luminescence of the powder compacts saturates at lower laser fluence (approximately 0.5 mJ $cm^{-2}$), while that of the single crystals saturates at 4 mJ $cm^{-2}$.

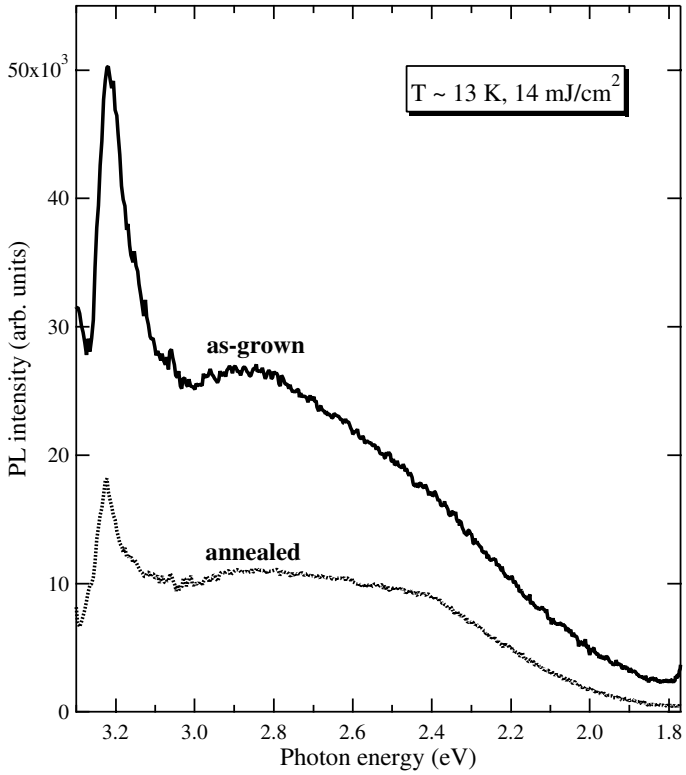


**Figure 12.** The photoluminescence spectra of the as-grown dark blue and annealed transparent $SrTiO_3$ crystals at about 13 K under an intense 355 nm photoexcitation (laser fluence = 14 mJ $cm^{-2}$).

## 4. Discussion

### *4.1. The reversible photo-induced spectral change*

The present experimental results on the reversible photo-induced spectral change of $SrTiO_3$ single crystal may be summarized as follows.

(1) The photo-induced reversible spectral change between weak PL and intense PL can be observed at different temperatures, from 13 K to room temperature. The spectral change takes time. The speed of the spectral change is nearly independent of temperature but it increases with increasing light intensity.
(2) The spectral change tends to saturate at a long light irradiation time (more than 90 min).
(3) The spectral change is induced by changing the specimen atmosphere between oxygen gas and vacuum only under a CW 325 nm laser light. On the other hand, intense pulsed 355 nm laser light (14 mJ $cm^{-2}$) never induced such spectral change.
(4) After removing the 325 nm laser light irradiation, each PL property persists for a long time even at room temperature under room light, regardless of any changes of atmosphere.

The result (1) indicates that the observed photo-induced spectral changes are purely electronic phenomena and they are not phonon-assisted ones. The result (1) indicates also that the B luminescence is an extrinsic luminescence due to the luminescence centres introduced

by a CW 325 nm laser light. Since the 325 nm (=3.81 eV) laser light never dissociates directly free $O_2$ molecules, the result (3) indicates that the phenomena arise from the photo-induced associative detachment and photo-induced dissociative adsorption of $O_2$ molecules near the $SrTiO_3$ surface. In this case, photoexcited $SrTiO_3$ crystal acts as a photocatalyst for decomposing $O_2$ molecules and also as an oxygen reservoir. The results also summarize how spectral change arises naturally from photo-activated oxidation and reduction.

Although some chemical heterogeneity on the surface has been pointed out for the surfaces of $SrTiO_3$ crystal reduced and oxidized at high temperatures (Szot *et al* 1997, Szot and Speier 1999), we discuss tentatively the observed photo-induced spectral changes at room temperature by regarding the measured $SrTiO_3$ crystal as chemically homogeneous, as follows. The chemical heterogeneity effects will be discussed in the next subsection. The reduction of the $SrTiO_3$ surface under a CW 325 nm laser light in vacuum may be accompanied by the creation of electron-captured oxygen vacancies $V_O''$, as follows:

$$(O^{2-} \text{ in lattice}) + (\text{CW 325 nm photon}) \rightarrow V_O'' + (\text{two electrons}) + \tfrac{1}{2}O_2, \quad (4)$$

where Kröger–Vink notation is used (Kröger and Vink 1956). Using a local spin density approximation plane wave pseudopotential method, Astala and Bristowe (2001) have shown that the doubly positively charged state is the most stable. This is in good agreement with the experimental result that oxygen deficiency in $SrTiO_3$ enhances the electrical conductivity (Jourdan and Adrian 2003) even at low temperatures. This means that most of the electrons around oxygen vacancies are released and, therefore, such oxygen vacancy sites are relatively positively charged. Therefore, the oxygen vacancies tend to trap photo-generated electrons. On the other hand, several authors (Henrich *et al* 1978, Cord and Courths 1985, Kimura *et al* 1995) proposed another type of defect at the $SrTiO_3$ surface as follows:

$$(O^{2-} \text{ in lattice}) + (\text{CW 325 nm photon}) \rightarrow (Ti^{3+}\text{–}V_O''\text{–}Ti^{3+}) \text{ complex} + \tfrac{1}{2}O_2. \quad (5)$$

In the complex, the $Ti^{3+}$ ions act as hole traps, while the vacancy $V_O''$ tends to trap electrons. For $SrTiO_3$ crystal, it is known that electrons determine the transport properties, for example, electrical conductivity and photoconduction, well, while no phenomena related to holes have been observed. This indicates that holes are almost trapped around crystal defects. Incidentally, the high dielectric constant (several tens of thousands) of $SrTiO_3$ crystal suppresses, creating excitons (ex). Toyozawa (1983) proposed three types of symmetry-breaking instability for excitons in the phonon field and, when the electron and the hole have deformation potentials of opposite sign, decomposition into a pair of self-trapped particles occurs. In other words, the instability of an exciton leads to lattice decomposition into an electron centre (an anion vacancy) $S_e$ and a hole centre (an anion interstitial) $S_h$, if the exciton is formed in the bulk. On surfaces, the hole centre is emitted from the surface, thus leaving only the electron centre. Therefore, such exciton instability may result in oxygen desorption at $SrTiO_3$ surfaces in vacuum and the oxygen vacancies thus produced give rise to B luminescence. Similar desorption has already been discussed for photo-induced breaking of the Si–O bond in a silica (Shluger and Stefanovich 1990). By a quantum chemical calculation, Eglitis *et al* (2004) has demonstrated that the chemical bonding of the perovskite structure contains a considerable covalent component, like the case for silica. It is noted that CW 325 nm laser light is indispensable for spectral change due to the photo-induced oxidation and reduction in $SrTiO_3$. The CW laser fluence in the present experiments was at most 0.8 W $cm^{-2}$, and therefore any bond-breaking mechanism based on the instability under high density excitation may be excluded from the present discussion. Unlike the case for alkali halides, a single interband excitation never induces the desorption of surface atoms in semiconductors, since the binding energy of atoms is larger than the energy gap. In such photoexcited semiconductor

cases, only atoms around crystal defects at the surfaces can be released (Puchin *et al* 1993, Itoh *et al* 1995, Itoh 1995, Itoh and Stoneham 2000, Song and Williams 1993). Astala and Bristowe (2001) calculated the oxygen vacancy formation energy of about 7 eV, which is approximately twice the bulk energy gap and slightly smaller than twice the CW 325 nm He–Cd laser photon energy, at the $TiO_2$-terminated (100) surface of $SrTiO_3$. Both the oxygen defects (for example, $Ti^{3+}$–$O''_V$–$Ti^{3+}$ and $O''_V$) inherent to $SrTiO_3$ surfaces and the infinite continuity of the laser light may enable the 325 nm laser photons to release $O_2$ molecules from the surface. Incidentally, pulsed 355 nm laser light (the pulse width is 4–5 ns), although the photon energy is close to that of the CW 325 nm laser light, never induced spectral change even at 14 mJ $cm^{-2}$, as a result of (3). Besides the surface defects, a small amount of $OH^-$ ions introduced inevitably during crystal growth by the Verneuil method should also be taken into account for the photo-induced spectral change. Incidentally, Ohmukai *et al* (1999) have observed a 126 nm laser-induced bond breaking and some polycrystalline precipitates on a $SiO_2$ glass. We could not detect any light scattering due to precipitates on the 325 nm laser light irradiated $SrTiO_3$ crystal.

It has been said that the desorption via such an excited state occurs within $10^{-13}$ s after laser pulse incidence. However, it is found that a relatively long time (more than 90 min) is taken to complete the spectral change in $SrTiO_3$, as a result of (2). This indicates that the photo-induced oxygen desorption probability is very low at the $SrTiO_3$ surface. The observed saturation tendency with further increasing $t_{ir}$ suggests that photo-induced oxygen defects increase the potential energy of the light irradiated surface. In such a case, equilibrium may be realized in a system composed of matter ($SrTiO_3$ crystal) and a radiation field. It can be assumed that the intensity, coherency and continuity of laser light determine the degree of fluctuation in the system and the dynamics of photo-induced spectral change. Unlike the case for a pulsed laser light, the possibility of successive electronic excitation is not ignored for CW laser light. More detailed experiments with varying frequency, pulse width and duty ratio of a periodic laser light pulse are in progress in our laboratory.

In relation to the UV laser light-induced oxygen defects and white luminescence, it should be noted that the crystals (for example, $LaAlO_3$) grown by light heating methods (for example, the floating zone methods and the arc furnace method) display intense white luminescence. During the growth, the crystals are exposed to intense ultraviolet radiation and, therefore, oxygen defects may be produced, exhibiting oxygen defect-related white luminescence between 3 and 2 eV (Kawabe *et al* 2000).

### *4.2. The B luminescence band*

The present experimental results on the B luminescence of $SrTiO_3$ single crystal may be summarized as having the following features.

(1) The broad B luminescence band is observed well under band-to-band excitation (>3.27 eV) in $SrTiO_3$ with a large energy shift (0.80 eV). Although the quantum yield is small, the B luminescence is also observed under a 442 nm (=2.80 eV) laser light excitation.
(2) The B luminescence intensity is considerably increased by photo-induced reduction with 325 nm (=3.81 eV) laser light irradiation in vacuum.
(3) The PL intensity increases with progressive annealing in a reducing atmosphere. The intensity peak energy and spectral width of the B luminescence depend on annealing history.
(4) The B luminescence decay curve consists of at least four components. The phosphorescence component lasts for at least several seconds. It is hard to fit the decay curve uniquely to a power law time ($t^{-2}$) dependence.

(5) With increasing temperature, the B luminescence intensity decreases, increasing the NBE and A luminescence bands. The B luminescence of both the single crystal and the powder compact disappeared above about 40 K.
(6) With increasing excitation intensity, the B luminescence intensity increases. On further increasing the excitation intensity, the B luminescence intensity attains a maximum at about 4 mJ $cm^{-2}$ and then decreases, increasing the NBE and A luminescence bands. The $SrTiO_3$ power compacts display the B luminescence intensity maximum at approximately 0.5 mJ $cm^{-2}$.

Feature (1) indicates that the B luminescence arises from several kinds of PL mechanisms. Both feature (2) and the feature (3) indicate that oxygen deficiency is a main cause of B luminescence. Feature (4) indicates that the deviation from stoichiometry creates different types of defect which give different luminescence centres and traps. Most workers have been studying $SrTiO_3$ crystals produced by the Verneuil method. Unfortunately, the compositional deviation of the crystals produced by the Verneuil method is known to be between $10^{-2}$ and $10^{-4}$ even for simple transition metal oxides (MnO, CoO, NiO and $TiO_2$). The chemical purities and isotope separation of the constituent elements (especially strontium and titanium) are not necessarily satisfactory and therefore most of the available $SrTiO_3$ crystals are at most 99.99% pure. These are problems common to many transition metal oxides. Moreover, since a flame consisting of $H_2$ gas and $O_2$ gas is used for the Verneuil crystal growth process, some contamination due to $OH^-$ ions may be inevitable. Feature (6) indicates that most of the B luminescence centres are at the specimen surface. Ignoring the above-described chemical impurity effects and noting only the effects due to the deviation from $SrTiO_3$ stoichiometry, we will discuss the results of the PL measurements.

We first discuss the excited states created in $SrTiO_3$ crystal by the third harmonics (355 nm) of the pulsed $Nd^{3+}$:YAG laser. Unlike CW 325 nm laser light, this 355 nm laser light never induced the spectral changes discussed in the previous subsection. The valence and conduction bands of $SrTiO_3$ mainly consist of the 2p orbits of $O^{2-}$ ions and the 3d orbits of $Ti^{4+}$ ions, respectively. Therefore, the fundamental absorption transfers the electron from the $O^{2-}$ ion to the $Ti^{4+}$ one. After such photoexcitation, some of the photo-produced electrons and holes recombine directly, displaying luminescence via some processes with short lifetime. However, perfect $SrTiO_3$ crystal is an indirect gap semiconductor and, therefore, the PL intensity is so weak that it cannot be measured. Another portion of electrons and holes may be trapped by intrinsic crystal defects at the surface and by the defects related to the deviation from the stoichiometry. In such a case, the PL property differs with the type of defect and also with the sites of defects, as follows.

*4.2.1. Oxygen defects at the surface and in the bulk.* Stashans and Vargas (2001) have calculated structural and electronic properties of the F centres (two electrons trapped by an oxygen vacancy) in $SrTiO_3$, as have Astala and Bristowe (2001). The results indicate that the wavefunctions of the two extra electrons extend over the titanium atoms closest to the two vacancies and over other nearby atoms, which is the same as the $Ti^{3+}$–oxygen vacancy complex model proposed by Henrich *et al* (1978), Cord and Courths (1985) and Kimura *et al* (1995). In other words, most of the oxygen vacancies are $Ti^{3+}$–oxygen vacancy complexes in real $SrTiO_3$ crystal. In this complex, $Ti^{3+}$ ion is one of the candidate hole-trapping centres and the oxygen vacancy is one of the candidate electron-trapping centres. Since electrical conduction due to holes is not observed, most of the photo-generated holes may be deeply trapped at $Ti^{3+}$ sites of the complexes. Unlike such holes, photo-generated electrons may be itinerant, experiencing repeatedly collisions with phonons and trapping by oxygen defects.

When some portions of photo-generated holes and electrons are trapped at distant complexes, a luminescence arises from accidental recombination of shallowly trapped electrons with distant holes localized around the defects, exhibiting a long lasting luminescence. Taking account of the electronic conductivity, both the absorption tail in the OD spectrum shown in the inset (a) of figure 2 and the energy difference of 0.80 eV may guarantee the existence of such deeply trapped hole states and shallowly trapped electron states. The broadness of the OD tail shown in the inset (a) of figure 2 suggests that such hole trap levels and electron trap ones arise from many slightly different defects. Using ultraviolet photoemission spectroscopy (UPS), Henrich *et al* (1978) found that the Fermi level of the fractured $SrTiO_3$ lies about 3 eV above the top of the valence band, which places it within 0.1 eV of the bottom of the conduction band. Also, they observed surface sensitive band gap emission band at energies between the top of the valence band and the Fermi level. These UPS results confirm also the existence of band gap states of the $SrTiO_3$ surface. Thus, the energy difference of 0.8 eV may correspond to the average energy difference between the shallow electron trap levels and the deep hole trap levels in the band gap. Since the observed luminescence decay curve was expressed as a multi-component exponential curve (at most four components), the overlapping between electron and hole wavefunctions is thought to be almost time independent.

With increasing laser fluence, the numbers of photo-generated electrons and holes increase and then the PL intensity may increase. With further increasing laser fluence, photo-generated electrons and holes become diffused more rapidly inside the crystal (bulk), and therefore the PL intensity decreases, as shown in figures 4(a) and (b). This is why the PL intensity maximum appears at 4 mJ $cm^{-2}$. In other words, this means that most of the defect luminescence centres are at the specimen surface. Since a powder specimen has a large specific surface area, a $SrTiO_3$ powder specimen may exhibit a PL intensity maximum at the laser fluence smaller than that of the single-crystal specimen. This suggestion was certainly confirmed by the present experimental result that the PL intensity maximum of the B luminescence for the powder compacts appeared at laser fluences (approximately 0.5 mJ $cm^{-2}$) lower than that (4 mJ $cm^{-2}$) observed for the single crystal. On the other hand, the luminescence arising from the defects in the bulk is thought to saturate at higher laser fluence. In addition to these defect effects, it should be taken into consideration that, at higher laser fluence, the recombination of photo-generated electrons and holes is enhanced and therefore it also reduces the luminescence intensity.

*4.2.2. Chemical heterogeneity in the surface region.* As stated in the previous sections, a colourless transparent $SrTiO_3$ single crystal is obtained by thermally annealing dark blue as-grown crystal at high temperature under an appropriate reducing atmosphere. Although it is colourless and transparent, the crystal is thought to be affected to some extent by such annealing treatment. In particular, it has been reported that the surfaces of reduced and oxidized $SrTiO_3$ contain not only the above-described oxygen defects but also Ruddlesden–Popper phases (Ruddlesden and Popper 1957, 1958). The combination of x-ray diffraction analysis with surface sensitive techniques has revealed a chemical inhomogeneity in the surface region of single crystals of $SrTiO_3$ prepared under low and high partial pressures of oxygen at elevated temperatures (Szot *et al* 1997). A solid state reaction leads to the formation of a multilayer-type structure. For oxidized crystals, they observed SrO-rich Ruddlesden–Popper phases at the surface and Magnelli phases of Ti in deeper layers of the surface region. The order of the layered structure is reversed for the reduced crystals, with Ti oxides of different oxidation levels at the surface and Ruddlesden–Popper phases in lower parts of the surface region. Measurements by atomic force microscopy are also reported for the (100) and (110) surfaces of $SrTiO_3$ single crystals prepared with different oxidizing and reducing conditions at elevated temperatures (1073–1273 K) (Szot and Speier 1999). The morphology of the surfaces turns

out to be drastically altered for both oxidized and reduced crystals in comparison with the original stoichiometric surfaces. The observed changes on the surface of $SrTiO_3$ due to the applied extensive thermal treatment cannot be explained by the formation of point defects, relaxation of the uppermost surface layer, rumpling or reconstruction due to vacancy ordering. Instead, the results have to be interpreted in terms of segregation processes and solid state reactions at elevated temperatures, which cause the formation of new chemical phases on the surface and in the region underneath. On the surface of oxygen-annealed $SrTiO_3$, this leads to the growth of steps perpendicular to the surface with step heights larger than the unit cell of the perovskite structure. Crystals prepared above 1173 K are shown to exhibit a step height of 1.18 nm which is attributed to the formation of a Ruddlesden–Popper phase $SrO^*(SrTiO_3)_n$ with $n = 1$ on the surface. In the case of reduced crystals, the topographic changes on the surface are caused by the formation of Ti-rich phases such as TiO and $Ti_2O$ on the surface above 1173 K. The complex interplay of the processes at the surface for different temperatures, in particular its dependence on the details of the heat treatment, is discussed. The induced chemical heterogeneity of the surface and in the near-surface region is interpreted in terms of a kinetic demixing.

Certainly, as shown in figures 11(a) and (b), we observed complicated spectral change under CW 325 nm laser light irradiation in oxygen gas and vacuum for the as-grown $SrTiO_3$ crystal, which cannot be explained entirely by the simple oxygen point defect model. Since the as-grown crystal has a higher light absorption coefficient than the colourless annealed crystal, the observed spectral change may be more affected by the surface crystal defects, including the chemical heterogeneity (for example, Ruddlesden–Popper phases) in the surface region.

Bearing these chemical heterogeneities in mind, we have measured the PL properties of the as-grown crystal at different stages of annealing in a reducing atmosphere and also measured those of a colourless transparent stepped $TiO_2$-terminated $SrTiO_3$ crystal whose step height is 0.4 nm. The detailed results will be reported in a separate paper (Mochizuki and Fujishiro 2005). The results are summarized as follows. The low temperature PL spectral structures of these crystals are almost the same as those of the colourless transparent (100) faced crystal, apart from the PL intensity. However, with progressive annealing, the dark blue colour becomes weak, the intensities of the NBE, A and B luminescence bands decrease and the lower energy tail of the PLE for the B luminescence becomes weak. Moreover, the excitation laser fluence giving the B luminescence intensity maximum (we call this fluence $F_{max}$) increases with progressive annealing. Like that for the as-grown crystals, the $F_{max}$ for the stepped $TiO_2$-terminated $SrTiO_3$ crystal decreases considerably in comparison with the $F_{max}$ for the colourless transparent $SrTiO_3$ crystal. The observed change in $F_{max}$ may be due to the change in the probability of electron–hole pairs with surface defects arising from chemical heterogeneity. We have observed also at least five broad optical absorption bands at about 2.9 eV, about 2.4 eV, about 2.1, 1.6 eV and about 0.9 eV for the as-grown crystal at different annealing stages. The dark blue colour of the as-grown crystal is attributed to this spectral structure in which the blue colour wavelength range is a spectral window. With progressive annealing, these absorptions decrease in intensity. These optical absorption bands may be assigned to oxygen defects and some chemical heterogeneity (Szot *et al* 2002). The broad OD tail observed for the colourless transparent crystal is thought to be a trace from these absorption bands; see the inset (a) of figure 2 in the present paper and the figure 4 in the paper reported by Szot *et al* (2002). In order to clarify the optical excitation in the Ruddlesden–Popper phases, more detailed surface sensitive spectroscopic measurements (for example, reflectivity and PL measurements under total reflection conditions) and morphological and structural measurements for the as-grown crystals at different stages of annealing are now in progress in our laboratory.

Taking account of these studies on different kinds of defects in the real $SrTiO_3$ crystal grown by the Verneuil method, we thus assign the B luminescence band to the radiative decay of the crystal defect-related excited electronic states. Alternatively, it is theoretically assumed that a long lasting luminescence arises also from some forbidden transition, and therefore we cannot ignore the contribution from de-excitation of some triplet excited states. Previously, many workers have discussed the long lasting B luminescence on the basis of intrinsic self-trapped electronic (exciton) states, ignoring the effects of crystal defects. As discussed above, it should now be apparent that defect effects are important for such self-trapping, and more careful consideration of them is necessary for deducing the intrinsic nature of $SrTiO_3$ from experimental data.

### *4.3. The NBE and A luminescence bands*

Both the NBE luminescence and the A band luminescence have the following features:

($\alpha$) Both luminescences become prominent under higher excitation intensity and do not saturate under intense excitation (14 mJ $cm^{-2}$). They grow to the detriment of the B luminescence with increasing excitation intensity.

($\beta$) With increasing temperature, both luminescences become prominent to the detriment of the B luminescence and survive even at high temperatures. The spectral structures of the two luminescences at room temperature are hardly changed by changing the excitation laser wavelength from 325 to 355 nm.

($\gamma$) Both luminescences are considerably enhanced in the as-grown crystal.

($\delta$) Both luminescences appear near the band edge energy region and have very short decay times ($\ll$50 ns).

Feature ($\alpha$) indicates that both the NBE luminescence and the A luminescence arise not from a small number of impurities and crystal defects, but from numerous luminescent species. Feature ($\beta$) indicates also that the NBE and A luminescence centres are stable at high temperatures, without any thermal exhaustion. This feature indicates that both luminescences are assisted by phonons. Feature ($\gamma$) indicates that the luminescence is emission assisted by crystal defects. Together with the features ($\alpha$), ($\beta$) and ($\gamma$), feature ($\delta$) suggests that the two luminescences arise from the same origin and are assignable to some kind of electron–hole recombination emission assisted by crystal defects and phonons.

We discuss these luminescence bands from two different viewpoints as follows. The frequency shift of the NBE luminescence band from incident 355 nm laser light is about 2207 $cm^{-1}$. This is too large for assigning this band to non-resonant Raman scattering (Sirenko *et al* 1999). Non-resonant Raman scattering in a cubic centrally symmetric crystal is forbidden by the odd parity of the optical phonons of $F_{1u}$ symmetry, and therefore cubic $SrTiO_3$ crystal displays weak broad Raman spectrum due to second-order Raman scattering in which two phonons are involved in the scattering process. In the tetragonal phase below 105 K, the phonon mode splits into two Raman-inactive modes of $A_{2u}$ and $E_u$ symmetry. When crystal defects (impurities and vacancies) are introduced (Kleemann *et al* 1997) or when uniaxial external fields (electric field and stress) are applied (Akimov *et al* 2000, Worlock and Fleury 1967), these first-order Raman-inactive modes can be observed only below 1000 $cm^{-1}$. They cannot explain the observed large frequency shift (about 2207 $cm^{-1}$) of the NBE luminescence. On the other hand, since the photon energy of the incident 355 nm (=3.49 eV) laser light is close to the reported direct gap energy (=3.47 eV; Capizzi and Frova 1970) and the observed PLE edge energy (=3.26 eV), we have to take account of the resonant Raman scattering effects. In this case, the Raman spectrum may display several resonance lines due to the scattering by different phonons near the direct and indirect gap energies, together with other critical points of

the interband transitions (Cardona 1982). As is well known theoretically, the resonant Raman process involves effects due to different intraband and interband scatterings, which display a broad resonance. If we regard the NBE and A luminescences as a result of such resonance Raman scattering, the phonon energy may be estimated from the difference between the indirect band edge energy (PLE edge energy = 3.26 eV) and the NBE luminescence peak energy (= 3.23 eV): the estimated value is 30 meV (=242 $cm^{-1}$), which is comparable to the transverse optical phonon frequency. Further discussion on the basis of such resonant Raman scattering requires measurements at different incident wavelengths and information about the chemical heterogeneity and defect effects on the Raman scattering.

Next, we discuss the NBE and A luminescence bands as follows. The NBE and the A luminescences were seen even at high temperatures, and they do not exhibit any PL intensity saturation under higher excitation intensity. Although an explanation with so-called donor–acceptor pair (D–A pair) luminescence due to unwanted impurities is frequently given for the intense broad luminescence band with intensity peaks for semiconductors, such D–A pair luminescence related to inevitable impurities may saturate under intense photoexcitation because of the limited numbers of donors and acceptors. Moreover, the luminescence intensity decreases remarkably with increasing temperature. Moreover, such a luminescence spectrum for D–A pairs related to unwanted impurities is thought to be time resolved, since separations between donors and acceptors differ. Therefore, we can ignore the contribution from the impurity-related D–A pair luminescence in the present discussion.

Now, we note that, since ideal $SrTiO_3$ crystal has an indirect gap, the crystal does not exhibit directly any intense intrinsic edge emission. When crystal defects giving shallow levels are introduced at the surface, a PL process becomes possible. We note moreover that the NBE and A luminescence bands are observed even at high temperatures under intense excitation and that these luminescence bands are considerably enhanced for the as-grown crystal, as seen in figure 12. Therefore, we regard the observed NBE and A luminescence bands as defect-induced edge luminescence (emission) ones, in which processes different phonons are created. The NBE luminescence band having a shift of 242 $cm^{-1}$ may be assigned to one of the optical phonon lines. A zero-phonon line anticipated at 3.26 eV is thought to be buried in the rise of the A luminescence band. The full width at half-maximum (FWHM) of the NBE band is about 30 meV. Such a large FWHM is thought be due to some structural inhomogeneity and damping. It is noted that the A luminescence displays an almost smooth and continuous band. This suggests that, besides optical phonons, many longitudinal and transverse acoustic phonons are created during electron–hole recombination.

## 5. Conclusion and remarks

In summary, we have investigated the reversible PL spectral change and the basic PL properties of as-grown and annealed $SrTiO_3$ single crystals, together with sintered $SrTiO_3$ powder compacts, at different temperatures from 12 K to room temperature. Three luminescence bands, NBE, A and B, are observed around 3.2, 2.9 and 2.4 eV, respectively. The B luminescence intensity changes with CW 325 nm laser light irradiation in oxygen gas and a vacuum. This result indicates that the B luminescence is not intrinsic luminescence but results from radiative decays of the oxygen defect-related photoexcited states and the chemical heterogeneity in the surface region. The NBE and A luminescences remain at high temperatures and they do not saturate under high density photoexcitation (at least 14 mJ $cm^{-2}$). Their PL properties (temperature dependence, excitation intensity dependence and time dependence) suggest that the NBE luminescence and the A luminescence arise from the same origin. Taking account of crystal defects, the NBE and the A luminescence are discussed qualitatively from two

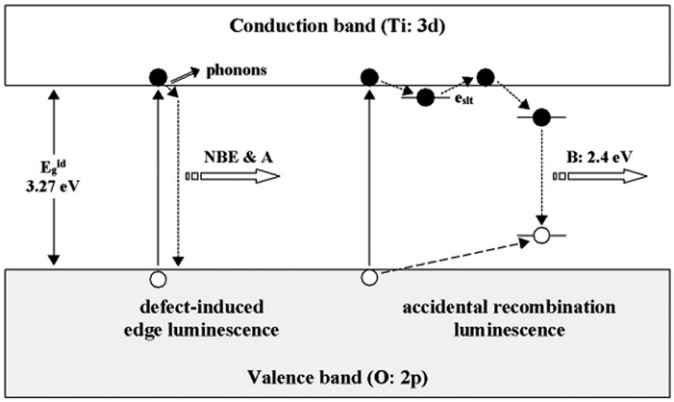


**Figure 13.** Some of the possible photoluminescence processes in real $SrTiO_3$ crystal. The solid arrow and dotted arrow indicate the optical absorption and radiative transition, respectively. The hollow arrow and double arrow indicate the luminescence and phonon creation, respectively. $E_g^{id}$ and $e_{slt}$ denote the indirect gap energy and the shallow electron trap level, respectively. For the accidental recombination model, the short dotted arrow and the broken arrow indicate the electron trapping and hole trapping, respectively.

different viewpoints: defect-induced resonant Raman scattering and defect-induced electron–hole recombination luminescence accompanying creation of phonons. At present, we do not exclude the possibility of other explanations. Although it constitutes a difficult problem, the surface defect structure and the defect-induced effects on the resonant Raman scattering and the edge luminescence (edge emission) should be considered in more detail.

A tentative energy diagram showing some of the possible PL processes in real $SrTiO_3$ crystal containing crystal defects is given in figure 13. The solid arrow and dotted arrow indicate the optical absorption and radiative transition, respectively. The hollow arrow and double arrow indicate the luminescence and phonon creation, respectively. $e_{slt}$ indicates a shallow electron trap. For the accidental recombination model, the short dotted arrow and the broken arrow indicate the electron trapping and hole trapping, respectively.

Incidentally, Pontes *et al* (2002) found intense PL in amorphous $SrTiO_3$ at room temperature under 488 nm (=2.539 eV) radiation from an $Ar^+$ ion laser. They ascribed the PL excited by low energy photons to non-bridging oxygen defects, for example, $TiO_5$. Study of how the non-bridging oxygen defects enhance the PL in amorphous $SrTiO_3$ is also helpful in discussing the PL properties of real $SrTiO_3$ crystal surfaces.

Finally, more detailed PL measurements, with excitation laser wavelengths varying around the band gap energies, on different annealing stages of $SrTiO_3$ crystals are now progress in our laboratory. Experiments with chopped laser light with different duty ratios on the reversible photo-induced spectral change are also now in progress. The results will be reported in a separate paper.

## Acknowledgments

This work was partially supported by a Grant-in-Aid for Scientific Research from the Ministry of Education, Science, Sports, Culture and Technology, Japan. This work was supported by an Interdisciplinary General Joint Research Grant for Nihon University. This work was also partially supported by a Project Research Grant from The Institute of Information Sciences of the College of Humanities and Sciences (Nihon University) and by a Cooperative Research Grant from The Institute of Natural Sciences (Nihon University).

## References


Akimov I A, Sirenko A A, Clark A M, Hao J-H and Xi X X 2000 *Phys. Rev. Lett.* **84** 4625
Astala R and Bristowe P D 2001 *Modelling Simul. Mater. Sci. Eng.* **9** 415
Blazey K W 1971 *Phys. Rev. Lett.* **27** 146
Capizzi M and Frova A 1970 *Phys. Rev. Lett.* **25** 1298
Capizzi M, Frova A and Dunn D 1972 *Solid State Commun.* **10** 1165
Cardona M 1965 *Phys. Rev.* **140** A651
Cardona M 1982 *Light Scattering in Solids II* (Berlin: Springer)
Cohen M I and Blunt R F 1968 *Phys. Rev.* **168** 929
Cord B and Courths R 1985 *Surf. Sci.* **162** 34
Eglitis R I, Kotomin E A and Borstel G 2004 *Comput. Mater. Sci.* **30** 376
Fujishiro F and Mochizuki S 2005 in preparation
Grabner L 1969 *Phys. Rev.* **177** 1315
Hasegawa T, Mouri S, Yamada Y and Tanaka K 2003 *J. Phys. Soc. Japan* **72** 41
Hasegawa T, Shirai M and Tanaka K 2000 *J. Lumin.* **87–89** 1217
Henrich V E, Dresselhaus G and Zeiger H J 1978 *Phys. Rev.* B **17** 4908
Itoh N 1995 *Butsuri* **50** 704 (in Japanese)
Itoh N, Kansaki J, Okano A and Nakai Y 1995 *Annu. Rev. Mater. Sci.* **25** 97
Itoh N and Stoneham A M 2000 *Material Modification by Electronic Excitation* (Cambridge: Cambridge University Press)
Jourdan M and Adrian H 2003 *Physica* C **388/389** 509
Katsu H, Tanaka H and Kawai T 2001 *J. Appl. Phys.* **90** 4578
Kawabe Y, Yamanaka A, Hanamura E, Kimura T, Takiguchi Y, Kan H and Tokura Y 2000 *J. Appl. Phys.* **88** 1175
Kimura S, Yamauchi J and Tsukada M 1995 *Phys. Rev.* B **51** 11049
Kleemann W, Albertini A, Kuss M and Linder R 1997 *Ferroelectrics* **203** 57
Kröger F A and Vink H J 1956 *Solid State Physics* vol 3 (New York: Academic) p 307
Mochizuki S 2003 *Physica* B **340–342** 944
Mochizuki S and Araki H 2003a *Physica* B **340–342** 913
Mochizuki S and Araki H 2003b *Physica* B **340–342** 969
Mochizuki S, Nakanishi T, Suzuki Y and Ishi K 2001 *Appl. Phys. Lett.* **79** 3785
Mochizuki S, Shimizu T and Fujishiro F 2003 *Physica* B **340–342** 956
Mochizuki S and Fujishiro F 2005 in preparation
Müller K A, Berlinger W and Tosatti E 1991 *Z. Phys.* B **84** 277
Müller K A and Burkard H 1979 *Phys. Rev.* B **19** 3593
Nasu K 2004 *Rep. Prog. Phys.* **67** 1607
Ohmukai M, Takigawa Y and Kurosawa K 1999 *Appl. Surf. Sci.* **137** 78
Pontes F M, Longo E, Leite E R, Lee E J H, Varela J A, Pizani P S, Campos C E M, Lanciotti F, Mastellaro V and Pinheiro C D 2002 *Mater. Chem. Phys.* **77** 598
Puchin V E, Shluger A L and Itoh N 1993 *Phys. Rev.* B **47** 10760
Ruddlesden S N and Popper P 1957 *Acta Crystallogr.* **10** 538
Ruddlesden S N and Popper P 1958 *Acta Crystallogr.* **11** 54
Shluger A and Stefanovich E 1990 *Phys. Rev.* B **42** 9664
Sirenko A A, Akimov I A, Fox J R, Clark A M, Li H C, Si W and Xi X X 1999 *Phys. Rev. Lett.* **82** 4500
Song K S and Williams R T 1993 *Self-Trapped Excitons* (Berlin: Springer)
Stashans A and Vargas F 2001 *Mater. Lett.* **50** 145
Szot K and Speier W 1999 *Phys. Rev.* B **60** 5909
Szot K, Speier W, Carius R, Zastrow U and Beyer W 2002 *Phys. Rev. Lett.* **88** 075508-1
Szot K, Speier W, Herion J and Freiburg C 1997 *Appl. Phys.* A **64** 55
Takesada M, Yagi T, Itoh M and Koshihara S 2003 *J. Phys. Soc. Japan* **72** 37
Toyozawa Y 1983 *Physica* B **112 & 118** 23
Tsang C and Street R A 1979 *Phys. Rev.* B **19** 3027
Worlock J M and Fleury P A 1967 *Phys. Rev. Lett.* **19** 1176
Zollner S, Demkov A A, Liu R, Fejes P L, Gregory R B, Alluri P, Curless J A, Yu Z, Ramdani J, Droopad R, Tiwald T E, Hilfiker J N and Woollam J A 2000 *J. Vac. Sci. Technol.* B **18** 2242